Draft version December 8, 2021
Typeset using LaTeX default style in AASTeX631

A Measurement of the Kuiper Belt's Midplane From Objects Classified By Machine Learning

Anonymous author(s)

(Received September 23, 2021; Revised December 8, 2021; Accepted Month ZZ, 202C)

Submitted to AJ

ABSTRACT

If the mean plane of the Kuiper Belt is the Laplace plane enforced by only the known planets, then warps in the Laplace plane at large semimajor axes may signal external perturbations such as unseen distant planets. We use a gradient boosting classifier to identify 2058 non-resonant Kuiper Belt objects in the semimajor axis range of 34.79–150 au, then compute their mean plane over that range and in distinct semimajor axis bins and estimate the error in each measurement with a random heuristic procedure. We find that the mean plane of the non-resonant Kuiper Belt is consistent with both the Laplace plane and the invariable plane of the solar system to greater than 3σ confidence except in the 40.525-42 au semimajor axis bin, just above the ν_{18} nodal secular resonance, where it is inconsistent with the Laplace plane, and in the 43-44 au bin, where it is inconsistent with the invariable plane. These results do not support the warp at semimajor axes above 50 au previously reported by Volk & Malhotra (2017).

Keywords: Kuiper Belt, Classical Kuiper Belt objects, Resonant Kuiper Belt objects

1. INTRODUCTION

Chiang & Choi (2008) posed the question: "If we could map, at fixed time, the instantaneous locations in three-dimensional space of all Kuiper Belt objects [KBOs], on what two-dimensional surface would the density of KBOs be greatest?" This surface, known as the mean plane or midplane of the Kuiper Belt, will be shaped by the unknown state of the Kuiper Belt at its formation and by the subsequent motion of planets inside the belt, passing stars outside, and any as-yet-unknown planets outside the belt. We may assume that, after billions of years, it is primarily determined by the secular effects of the planets. If the secular theory is well developed and the population of KBOs well surveyed, a measurement of mean plane may hold clues to as-yet-undiscovered outer planets. At present, the leading theory for the Kuiper Belt's midplane is the Laplace-Lagrange linear secular perturbation theory (Chiang & Choi 2008; Murray & Dermott 1999), or Laplace theory for short. This theory predicts the local normal as a function of semi-major axis. Its prediction, though not truly a flat plane, is known as the Laplace plane. An alternate candidate is the plane normal to the total orbital angular momentum of the solar system, known as the invariable plane (Souami & Souchay 2012).

Previous measurements of the Kuiper Belt midplane have produced inconsistent results. Brown & Pan (2004) report a mean plane of $(i_0, \Omega_0) = (1.86°, 81.6°)$, where i_0 and Ω_0 are respectively the mean plane's inclination and longitude of node. This is consistent with the Laplace plane at semimajor axis $a = 44$ au but inconsistent ($> 3\sigma$) with the invariable plane of the solar system as well as the (orbital planes of Neptune and Jupiter). Elliot et al. (2005), use five separate methods to compute Kuiper Belt planes, finding inclinations between $i_0 = 1.65°$ and $i_0 = 2.49°$, and longitudes of node between $\Omega_0 = 97.4°$ and $\Omega_0 = 104.0°$, with a preferred value of $(i_0, \Omega_0) = (1.51° \pm 0.26°, \Omega_0 = 100.0° \pm 8.8°)$. They reject the Laplace plane at 3σ confidence as the Kuiper Belt midplane, but do not reject the invariable plane. Chiang & Choi (2008) compute the midplane for two small samples of KBOs near $a = 38$ au and $a = 43$ au and conclude that they cannot reject either the Laplace plane or the invariable plane for either semimajor axis region. Volk & Malhotra (2017) find a midplane for the classical Kuiper Belt of $(i_0, \Omega_0) = (1.8°, 77°)$ for the sample of non-resonant KBOs in the semimajor axis range 42-48 au. Their midplane measurements at higher resolution in semimajor axis are consistent with either the Laplace plane or the invariable plane in the semimajor axis range of 35 au to 45 au (except for a warp near 40 au, due to a secular resonance), but strongly inconsistent with either plane beyond 50 au at

the 97%-99% confidence level. The most recent measurement of the Kuiper Belt's midplane, by Van Laerhoven et al. (2019), rejects the invariable plane within $a = 44.4$ au and does not reject the Laplace plane; beyond 44.4 au both planes are accepted. In the present work, we revisit the measurement of the Kuiper Belt's midplane using a different method to identify non-resonant KBOs, in the hope of resolving the controversy between past midplane measurements or addressing the apparent warp at high semimajor axes seen by Volk & Malhotra (2017). We use a gradient boosting classifier to identify 2058 non-resonant KBOs in the JPL Small Body Database as of 2021 December 4, compute their mean plane in semimajor axis ranges from 34.79 to 150 au using a method relatively insensitive to survey bias, and estimate the margin of error of those measurements using a random heuristic procedure.

2. LAPLACE PLANE

Though their measurements of the midplane differ, researchers including Volk & Malhotra (2017), Chiang & Choi (2008), and Brown & Pan (2004) agree that for low-eccentricity, low-inclination, non-resonant KBOs with perihelia outside the orbit of Neptune, the midplane is adequately described by Laplace theory as set forth in Murray & Dermott (1999). In this approximation, the planetary perturbations on a test particle are averaged over time, its semimajor axis stays constant, while the eccentricity, inclination and the orbit orientation angles vary with time. The inclination and longitude of node, paired as

$$\begin{aligned} q &= \sin i \cos \Omega \\ p &= \sin i \sin \Omega, \end{aligned} \tag{1}$$

define the "inclination vector," which is split into a sum of two parts,

$$\begin{aligned} q &= q_0 + q_1 \\ p &= p_0 + p_1, \end{aligned} \tag{2}$$

where $q_0 = \sin i_0 \cos \Omega_0$, etc. The forced elements (q_0, p_0) define the Laplace plane; these are defined by the instantaneous orbit planes of the planets and the masses of the planets. The free elements (q_1, p_1) precess around the Laplace plane at a fixed angular rate. The free inclination i_1 remains constant and the free longitude of node Ω_1 circulates. As the orbit plane of a KBO precesses around its local Laplace plane, it follows that the midplane of a large population of test particles in a small semimajor axis range (with dispersed orbit planes) is described by the Laplace plane, as shown in simulations by Murray & Dermott (1999) and Chiang & Choi (2008). Because the Laplace plane is defined by the instantaneous orbit planes of the planets, it varies with time and by semimajor axis location of the KBOs.

The Laplace plane in Figure 2 is computed according to the theory described in Murray & Dermott (1999), and using data for the J2000 ecliptic/equinox barycentric planetary elements retrieved from JPL Horizons for 2022 January 21 and planetary masses from Standish (1995). Laplace theory as set forth in Murray & Dermott (1999) and other sources describes the Laplace plane in heliocentric coordinates, rather than barycentric coordinates. The portion of the disturbing function used to develop the theory depends on eccentricity, inclination, longitude of node, longitude of pericenter, and semimajor axis. Only semimajor axis is affected by the heliocentric-to-barycentric conversion, and the short-period oscillations in heliocentric semimajor axis caused by the motions of planets interior to the Kuiper Belt average to zero over secular timescales. Barycentric coordinates, which lack those semimajor axis oscillations, are therefore more convenient and no less accurate than heliocentric coordinates for high-a Laplace plane calculations. As a practical matter, the Laplace plane for orbits outside Neptune's is nearly identical in heliocentric and barycentric coordinates except immediately near the secular resonance locations at (barycentric) semimajor axis values of 34.79 au and 40.524 au.

3. MEAN PLANE MEASUREMENT

Accurately measuring any population statistic from a limited sample requires understanding the limitations and biases of the sample, which in turn requires some prior knowledge about the general characteristics of the population and the sampling method.

Because the orbital angular momentum vector is normal to the plane of an individual orbit and the total orbital angular momentum vector is normal to the midplane of a group of orbits, it would seem obvious to simply average

the angular momenta of a group of KBOs to find their midplane. Without a fair or complete census, this method is unreliable, as it will reflect the biases of the observational surveys that produced the sample. Surveys limited in ecliptic latitude and longitude will yield measured midplanes biased toward the observed regions, whatever the true population midplane may be.

Brown & Pan (2004) argued that sky-plane velocity vectors

$$\hat{\boldsymbol{v}}_t = \hat{\boldsymbol{h}} \times \hat{\boldsymbol{r}} \tag{3}$$

may be used to find the unbiased midplane of a group of KBOs, where the barycentric unit angular momentum, $\hat{\boldsymbol{h}}$, and position, $\hat{\boldsymbol{r}}$, are found from the ICRF ecliptic latitude β, ecliptic longitude λ, inclination i, and longitude of node Ω as

$$\hat{\boldsymbol{h}} = \big(\sin i \sin\Omega, -\sin i \cos\Omega, \cos i\big), \tag{4}$$

$$\hat{\boldsymbol{r}} = \big(\cos\beta\cos\lambda, \cos\beta\sin\lambda, \sin\beta\big). \tag{5}$$

Volk & Malhotra (2017) describe a simple method for computing the midplane of a KBO population using the sky-plane velocity vectors. The sky-plane velocity, $\boldsymbol{v}_t$, of a KBO orbiting exactly on the midplane will always be normal to the midplane orbit normal, so that

$$\hat{\boldsymbol{n}} \cdot \hat{\boldsymbol{v}}_t = 0. \tag{6}$$

The midplane can then be computed as the plane whose orbit normal is *most* normal to the *most* KBO velocities, or the plane that minimizes

$$S = \sum_{i=1}^{N} |\hat{\boldsymbol{n}} \cdot \hat{\boldsymbol{v}}_{t,i}|, \tag{7}$$

where

$$\hat{\boldsymbol{n}} = \left(p_0, -q_0, \sqrt{1 - p_0^2 - q_0^2}\right). \tag{8}$$

The function S may be minimized on a grid search in (q_0, p_0) space for a computationally simple, if tedious, method of finding the midplane. Given a list of (q, p) for N_K KBOs, we find the minimum and maximum values of q and p in the list and compute S at all points $q_{\min} \le q \le q_{\max}$, $p_{\min} \le p \le p_{\max}$, with grid spacing $\Delta q = (q_{\max} - q_{\min})/1000, \Delta p = (p_{\max} - p_{\min})/1000$. This grid search method is applied to the KBOs identified as non-resonant using the gradient boosting classifier in section 5. The precision of the midplane fit is limited by the grid spacing, but the spacing is small compared to the confidence regions that are computed later. Volk & Malhotra (2017) showed that this method is not entirely bias-free when applied to synthetic KBO populations generated using biased synthetic surveys, but it is much more accurate than simply averaging the individual orbit normals from the same synthetic samples. The midplane (q_0, p_0) is trivially converted to an inclination and longitude of node (i_0, Ω_0).

4. MEAN PLANE MEASUREMENT UNCERTAINTY

We use a random heuristic procedure to estimate the uncertainty in each grid search estimate of the midplane (q_0, p_0) of a sample of N_K observed non-resonant KBOs. This procedure is simplified from the corresponding method in Volk & Malhotra (2017). We generate a new list of N_K synthetic objects and repeat N_R times. This produces a list of N_R resampled midplanes $(q_{0,r}, p_{0,r})$, where $1 \le r \le N_R$. Although it is possible to simply transform the resampled midplanes $(q_{0,r}, p_{0,r})$ to $(i_{0,r}, \Omega_{0,r})$ and directly compute their percentiles, this is discouraged for three reasons. First, there are several methods of computing percentiles that may slightly alter the results. Second, longitude of node is defined on a circular domain, making the usual idea of a percentile less meaningful and requiring alternative circular statistics. Third, computing separate percentile intervals for inclination and longitude of node ignores any correlations between resampled $q_{0,r}$ and $p_{0,r}$. Instead, we compute a 1σ covariance ellipse from the $(q_{0,r}, p_{0,r})$ and take the maximum and minimum values of i_0 and Ω_0 on the ellipse as the 1σ confidence intervals for the inclination and longitude of node

of the Kuiper Belt midplane. This preserves some sense of the correlation between q and p. If the ellipse surrounds the origin, the confidence interval for Ω_0 spans the entire circle.

In each of N_R repetitions, the ith synthetic object is found by randomly selecting the jth real object from the KBO sample and choosing a_i uniformly from the range $0.99a_j - 1.01a_j$ and e_i uniformly from the range $0.95e_j - 1.05e_j$. We assign the mean anomaly and argument of pericenter uniformly from the circle. The total inclination vector (q_i, p_i) is found as the sum of the free and forced inclination vectors,

$$(q_i, p_i) = (q_0, p_0) + (q_{1,i}, p_{1,i}), \tag{9}$$

where the forced inclination vector (q_0, p_0) is the grid-search midplane of the KBO sample and the free inclination vector $(q_{1,i}, p_{1,i})$ is a pair of uncorrelated zero-mean Gaussian random variables with $\sigma_q = \hat{\sigma}_q$, $\sigma_p = \hat{\sigma}_q$. That is, the standard deviations in q and p for the free inclination vector are taken from the KBO sample. This approximates the common technique of modeling KBO inclinations with a sum of Rayleigh distributions and KBO longitudes of node with a uniform distribution on the circle, without conducting a complicated model fit for each semimajor axis bin. The ecliptic latitude β_i and ecliptic longitude λ_i of the object are then computed.

In each repetition, synthetic objects are generated until there is exactly one synthetic (β_i, λ_i) pair for each real (β, λ) pair in the KBO sample, where, as in Volk & Malhotra (2017), an acceptable match is within one degree in β and within five degrees in λ. This method approximates the combined biases of all surveys that contributed to a KBO sample without making complicated assumptions about any individual survey. However, some real KBOs are difficult to match using this method, so we set a maximum iteration count of 10^7 to move past troublesome objects. In fact, all objects converged within the 10^7 iteration limit on every repetition. For each bin, $N_R = 40,200$ random resampling repetitions are used, which allows the 1σ covariance ellipses in p and q to reliably converge to the precision to which we report the results, as shown in Figure 1 for the 1σ lower bound of the mean plane inclination for the 34.79-150 au bin. Convergence plots for the inclination and longitude of node upper and lower bounds for each bin are similar and we omit the others for brevity, though they are available upon request.

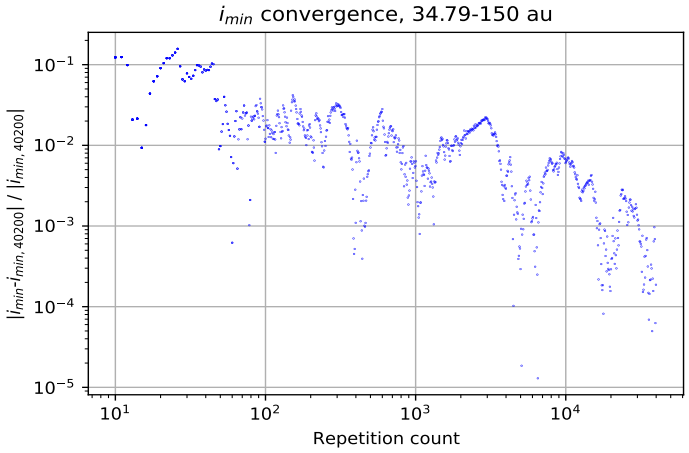

Figure 1. After 40,000 repetitions of the heuristic sampling process, the 1σ lower bound for the inclination of the mean plane of the 34.79-150 au bin has converged to a fractional variation of less than 10^{-3}, so we report the resulting inclination bound to two significant figures in Table 3.

This procedure for generating sets of synthetic objects from the observed dataset is driven by the desire to use as many real observed objects as possible in the mean plane computation, balanced against the reality that the complete catalog of observed objects does not come from a single well-characterized survey. This prevents us from applying systematic debiasing procedures to the observed catalog, and instead we make the key assumption that each patch of sky in ecliptic coordinates has been thoroughly observed, such that a true population will have the same number of objects in each patch of sky as the observed catalog. Our randomized procedure for generating synthetic objects satisfies this assumption and crudely controls for brightness and magnitude by requiring the semimajor axis and eccentricity of each synthetic object to be close to that of a real object.

5. RESONANT OBJECT IDENTIFICATION

Laplace theory is developed assuming that no two planets in the system are in mean motion resonances (MMRs) with each other, and no test particle is in a mean motion resonance with any planet. Before the midplane of any KBO population can be compared with the Laplace plane, all resonant KBOs must be identified and removed.

The most reliable method for identifying resonant KBOs from a sample population is to integrate the orbit of each KBO in a reliable n-body integrator with perturbations from all the planets, recording all the resonant angles of interest. The orbit must be integrated long enough to allow the longest-period resonant angles to librate, which often requires tens of millions of years. For the longest-period angles, for angles that librate over large fractions of the circle, or for objects that alternate between libration and circulation, it may be difficult to distinguish resonant objects from non-resonant objects. Uncertainty in KBO orbital elements can also complicate resonant classification. Because new telescopes are expected to dramatically increase the number of known KBOs in the upcoming decade, it is desirable to have a more efficient way to classify KBOs without 10+ Myr integrations.

Smullen & Volk (2020) used the criteria of Gladman et al. (2008) to classify 2305 KBOs from the Minor Planet Center database as of 2016 October 20 after fitting new orbits to each object and integrating them for 10 Myr. For ease of use, Smullen & Volk (2020) provide Python code to classify an object from its MPC identification or from its orbital elements. These tools integrate the orbit in the n-body integrator Rebound for 100 kyr and record 55 features for the gradient boosting classifier. The classifier assigns the particle separate probabilities of being either Classical, Scattering, Detached, or Resonant; the class with the highest probability is the reported category. The probabilities assigned sum to 100%.

To generate a set of non-resonant KBOs for which to calculate the mean plane, we used the JPL Solar System Dynamics Group's Small Database Query to retrieve all objects with constraints of heliocentric $34 < a < 150$ au, $q > 30.07$ au (the semimajor axis of Neptune), $e < 1$. On 2021 December 4, this returned 3544 objects with heliocentric elements at the epoch 2022 January 21. We eliminated all objects without specified semimajor axis uncertainty or with fractional semimajor axis uncertainty $\delta a/a > 5\%$, leaving 2860 objects. Next, we downloaded the MPCORB.DAT database from the Minor Planet Center on 2021 December 4 and cross-referenced it against the Solar System Dynamics database to eliminate all objects that have been observed for fewer than the three oppositions recommended by Gladman et al. (2008), leaving 2748 objects.

To classify the remaining objects, we downloaded the Python sample code and training data **KBO_features.csv** from the Smullen & Volk (2020) GitHub repository. We used their gradient boosting classifier without modification and trained it on the same training set they provided. We emphasize that we operated their gradient boosting classifier as an unmodified black box. Any readers with questions about the development, application, validity, or operation of this classifier should consult Smullen & Volk (2020); we feel it unnecessary to present that information in detail here. Because the gradient boosting classifier requires barycentric elements, we used Astroquery to retrieve barycentric elements at 2022 January 21 from Horizons.

Given the uncertainties in many KBO orbits, it is possible that the nominal Horizons orbit will result in an incorrect classification for some objects. To allay this concern, we download the 6x6 covariance matrix for each remaining object from the Small Body Database API and use it to generate 300 clones for each object from a Gaussian distribution centered at the nominal orbit. This covariance matrix is not computed for the same epoch of 2022 January 21, but we neglect to compute a new covariance matrix for the epoch. If over 50% of these clones (150 objects) are classed as Resonant, we discard the object. A firm classification as Classical, Scattering, or Detached is not needed for our mean plane computations, so we do not further examine the classifications of the clones. The mean planes in each semimajor axis bin are then computed using the nominal orbits of the remaining 2058 objects. The complete set of classified KBOs with semimajor axes between 34.79 and 150 au is provided online. A small sample is shown in Table 1. The lower bound of 34.79 au is chosen because it is just above a secular resonance.

6. RESULTS AND DISCUSSION

With the data and methods described above, the midplanes and confidence intervals we found are shown in Table 3 and plotted in Figure 2. The semimajor axis-varying Laplace plane is plotted in blue, and the invariable plane is indicated by the black horizontal line. The best-fit midplane results reported in Table 3 are plotted in brown, where the horizontal error bars indicate the width of the semimajor axis bin and the vertical error bars indicate the

Table 1. Sample Table of Classified KBOs

MPC packing	Nominal	Most common	Detached	Scattering	Classical	Resonant
59358	Scattering	Scattering	0	261	37	3
B8378	Resonant	Classical	0	0	152	149
B9068	Scattering	Scattering	73	214	0	14
C9972	Classical	Classical	0	0	301	0
D1318	Resonant	Resonant	0	0	0	301

NOTE—Classified KBOs from 34-150 au as of 2022 January 21. The nominal orbit plus 300 clones generated from the 6x6 Gaussian covariance envelope are separately classified.

Table 2. Non-Resonant KBO Counts

Semimajor axis bin, au	Count
34.79-40.524	179
40.524-42	149
42-43	215
43-44	394
44-45	281
45-48	408
45-50	448
50-80	296
50-150	392
Total (34.79-150)	2058

1σ confidence interval. For comparison, the results of Volk & Malhotra (2017) are plotted in magenta, with a small offset in the semimajor axis location of the vertical line for legibility. Separately, Figure 3 shows the 1σ, 2σ, and 3σ confidence ellipses in the (q_0, p_0) plane for each semimajor axis bin, as described in Section 4. The best-fit midplane is shown as a brown +, with the invariable plane represented by a black x, the J2000 ecliptic/equinox pole by the origin, the semimajor axis-varying Laplace plane by a blue line, and the best-fit midplane from Volk & Malhotra (2017) by a magenta diamond. Note that Volk & Malhotra (2017) generated (q, p) for synthetic samples using a model population centered at the Laplace plane, whereas we generate (q, p) for synthetic samples using the standard deviations in q and p of the observed bins and use the best-fit observed midplane as the central (q, p). Simple acceptance/rejection decisions are shown for each bin in Table 4.

We note two semimajor axis bins whose boundaries are slightly different in our work compared with previous literature. Previous lists of KBO counts and necessary repetitions per semimajor axis bin have used low-a bin boundaries of 35 au and 40.3 au to conform with prior work by Volk & Malhotra (2017). The results in this section use low-a bin boundaries of 34.79 au and 40.524 au, as these are the secular resonance locations computed from J2000 barycentric planetary elements for 2022 January 21.

For all but two semimajor axis bins, we do not reject either the Laplace plane or the invariable plane as the true midplane at the 3σ level. The two exceptions are as follows. For the 40.524-42 au bin, the Laplace plane is rejected at a 3σ confidence level but the invariable plane is not. For the 43-44 au bin, the invariable plane is rejected at 3σ confidence but the Laplace plane is not.

Table 3. KBO Midplane 1σ Confidence Intervals (Degrees)

Semimajor axis bin, au	i^-	i_0	i^+	Ω^-	Ω_0	Ω^+
34.79-40.524	0.5	2.4	4.4	100	152	202
40.524-42	4.8	7.1	9.8	251	271	290
42-43	0.3	1.5	2.7	360	52	112
43-44	1.4	2.1	2.7	74	94	113
44-45	1.2	1.9	2.6	64	95	111
45-48	0.2	1.2	2.3	302	0	57
45-50	0.4	1.4	2.5	309	355	40
50-80	1.0	0.9	2.7	0	47	360
50-150	0.5	1.0	2.6	0	110	360
Total (34.79-150)	1.1	1.5	2.0	63	82	101

Table 4. Invariable Plane (IP) and Laplace Plane (LP) Checks

Semimajor axis bin, au	IP, 1σ	IP, 2σ	IP, 3σ	LP, 1σ	LP, 2σ	LP, 3σ
34.79-40.524	...	✓	✓	✓	✓	✓
40.524-42	...	...	✓	...	...	...
42-43	...	✓	✓	✓	✓	✓
43-44	...	...	...	✓	✓	✓
44-45	...	...	✓	✓	✓	✓
45-48	...	✓	✓	...	...	✓
45-50	...	✓	✓	...	...	✓
50-80	✓	✓	✓	✓	✓	✓
50-150	✓	✓	✓	✓	✓	✓

NOTE—Acceptance/rejection decisions for invariable plane and Laplace plane by semimajor axis bin, 2021. Checks are accepted, ellipses are rejected.

Chiang & Choi (2008) computed the Kuiper Belt plane, with an uncertainty estimate, for 10 objects with $38.09 < a < 39.10$ au, and for 80 objects with $42.49 < a < 43.50$ au. They fail to rule out either the Laplace plane or the invariable plane as the true Kuiper Belt plane in those semimajor axis ranges with greater than 3σ confidence. We have not computed the Kuiper Belt plane and its uncertainty specifically for either range, but our results in the 34.79-40.524 au, 42-43 au, and 43-44 au bins seem consistent with their results for the 38.1-39.1 au and 42.5-43.5 au bins.

Van Laerhoven et al. (2019) computed the plane of the cold classical Kuiper Belt, with uncertainties, for 107 objects in the 42.4-43.8 au bin, 82 objects in the 43.8-44.4 au bin, and 67 objects in the 44.4-47.0 au bin. Also, they computed the Kuiper Belt plane, with uncertainties, for 57 objects in the 50-80 au bin and for 83 objects in the 48-150 au bin. In the 42.4-43.8 au and 43.8-44.4 au bins, they reject the invariable plane at 99% confidence and accept the Laplace plane. In the high-a bins, the Laplace plane is rejected at 99% confidence and the invariable plane is accepted. Our results are broadly similar for low a, except for slight differences in the confidence level at which the invariable plane is rejected, but at high a we do not reject the invariable plane. Our results differ from Brown & Pan (2004) and Elliot et al. (2005), each of whom reject one or the other of the Laplace plane and the invariable plane.

Since our method is based on that of Volk & Malhotra (2017), we comment in more detail on the differences between those results and ours. Our results are consistent with their conclusions within 50 au, but we do not detect the strong warp they report at $a > 50$ au. Instead, our results show that the midplane inclination above 50 au is constrained to low values consistent with the Laplace plane and the invariable plane, while the (q_0, p_0) spread in simulated resampled

midplanes is large enough to surround the origin, making the midplane's nodal direction entirely uncertain. We conjecture that the different results at large semimajor axes may be due to sample selection. It is conceivable that their method, which manually examined resonances up to 30th order, may have systematically rejected distant low-inclination objects in higher-order resonances that were not detected by the gradient boosting classifier. The inclusion of these "false positives" would tend to drive down the midplane inclination and randomize the midplane longitude of node.

Our inclusion of scattering objects might also partially account for the lower mean inclinations and unconstrained mean longitudes of node for $a > 50$ au. Scattering objects are often distant and highly inclined, but their longitudes of node vary widely, such that their mean plane might have nearly zero inclination. This could significantly affect the midplane at high a, where classical non-resonant objects are relatively few.

We also observe minor differences in the 34.79-40.524 au bin and the 40.524-42 au bin. In the 34.79-40.524 au bin, we compute a best-fit midplane whose inclination and longitude of node are very close to those of Volk & Malhotra (2017). Our 1σ inclination margin of error is of similar size to theirs, but is just enough smaller that the 1σ (q_0, p_0) covariance ellipse no longer encircles the origin (though that is hard to see in Figure 3). This makes a unique determination of the longitude of node possible in Figure 2 and Table 3 at the 1σ level, but the longitude of node is still not uniquely determined at the 2σ or 3σ levels. In the 40.524-42 au bin, we compute a best-fit midplane that is much closer to the Laplace plane than in the 2017 paper, though it still differs by 3σ in the (q_0, p_0) plane. We conjecture that, with future increases in the size of KBO samples, splitting this bin into two or more narrower semimajor axis ranges would enable higher precision comparisons of the measured and predicted Laplace plane for each new bin, as there would be less Laplace plane warpage in each bin. Because Laplace theory assumes small perturbations, its predictions are generally less reliable near secular resonances.

We close by emphasizing that each study cited uses different methods to select which objects to include in a mean plane calculation, to compute the mean plane, and to estimate the uncertainty of the result. Ours is one of the simplest methods, conceptually and computationally. Future increases in the observational sample sizes will enable higher confidence results in measurements of the Kuiper Belt midplane, and should be examined for their potential to detect the effects of unseen distant planets or other unmodelled perturbations.

(Acknowledgments anonymized for review)

Software: astroquery (Ginsburg et al. 2019), rebound (Rein & Liu 2012), scikit-learn (Pedregosa et al. 2011), shapely (Gillies et al. 2007–)

REFERENCES

Brown, M. E., & Pan, M. 2004, The Astronomical Journal, 127, 2418

Chiang, E., & Choi, H. 2008, The Astronomical Journal, 136, 350

Elliot, J., Kern, S., Clancy, K., et al. 2005, The Astronomical Journal, 129, 1117

Gillies, S., et al. 2007–, Shapely: manipulation and analysis of geometric objects. https://github.com/Toblerity/Shapely

Ginsburg, A., Sipőcz, B. M., Brasseur, C. E., et al. 2019, AJ, 157, 98, doi: 10.3847/1538-3881/aafc33

Gladman, B., Marsden, B. G., & VanLaerhoven, C. 2008, The Solar System Beyond Neptune, 43

Murray, C. D., & Dermott, S. F. 1999, Solar System Dynamics (Cambridge University Press)

Pedregosa, F., Varoquaux, G., Gramfort, A., et al. 2011, Journal of Machine Learning Research, 12, 2825

Rein, H., & Liu, S. F. 2012, A&A, 537, A128, doi: 10.1051/0004-6361/201118085

Smullen, R. A., & Volk, K. 2020, Monthly Notices of the Royal Astronomical Society, 497, 1391

Souami, D., & Souchay, J. 2012, Astronomy & Astrophysics, 543, A133

Standish, E. M. 1995, Highlights of Astronomy, 10, 180

Van Laerhoven, C., Gladman, B., Volk, K., et al. 2019, The Astronomical Journal, 158, 49

Volk, K., & Malhotra, R. 2017, The Astronomical Journal, 154, 62

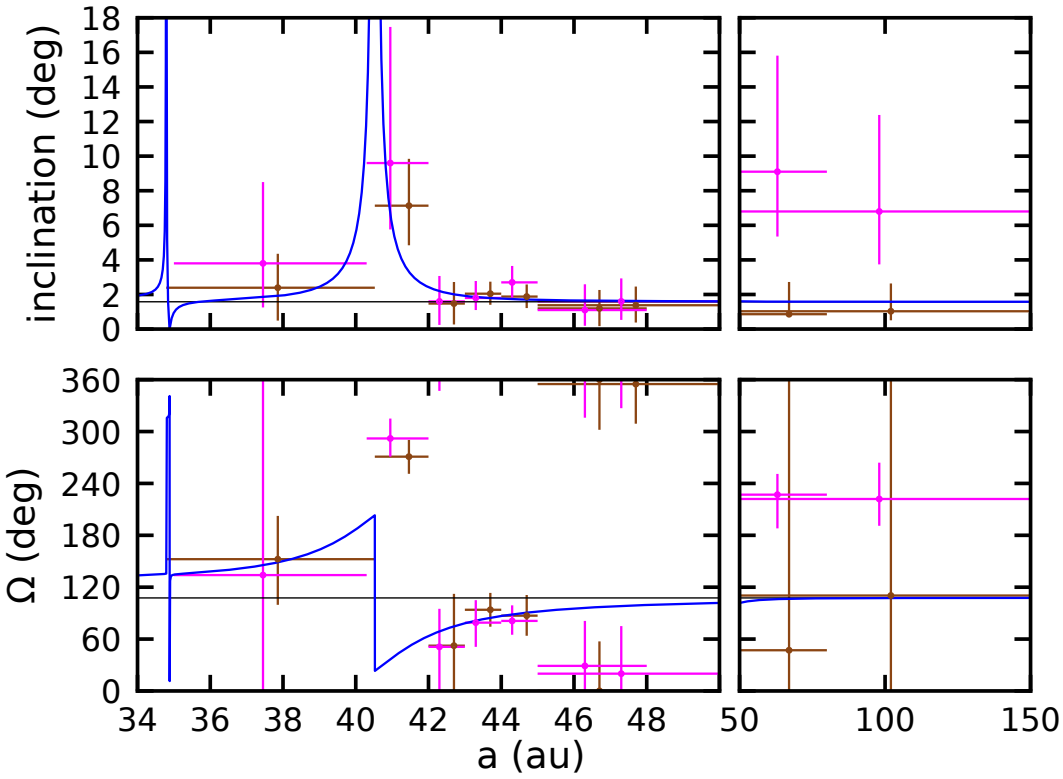

Figure 2. Kuiper Belt midplane and 1σ confidence intervals by semimajor axis bin. The semimajor axis-varying Laplace plane is blue. The invariable plane is a horizontal black line. The best-fit midplanes and confidence intervals from Volk & Malhotra (2017) are in magenta, and those from this work are in brown. For the sake of readability, the vertical magenta and brown lines have been slightly offset from each other in semimajor axis when they would otherwise overlap.

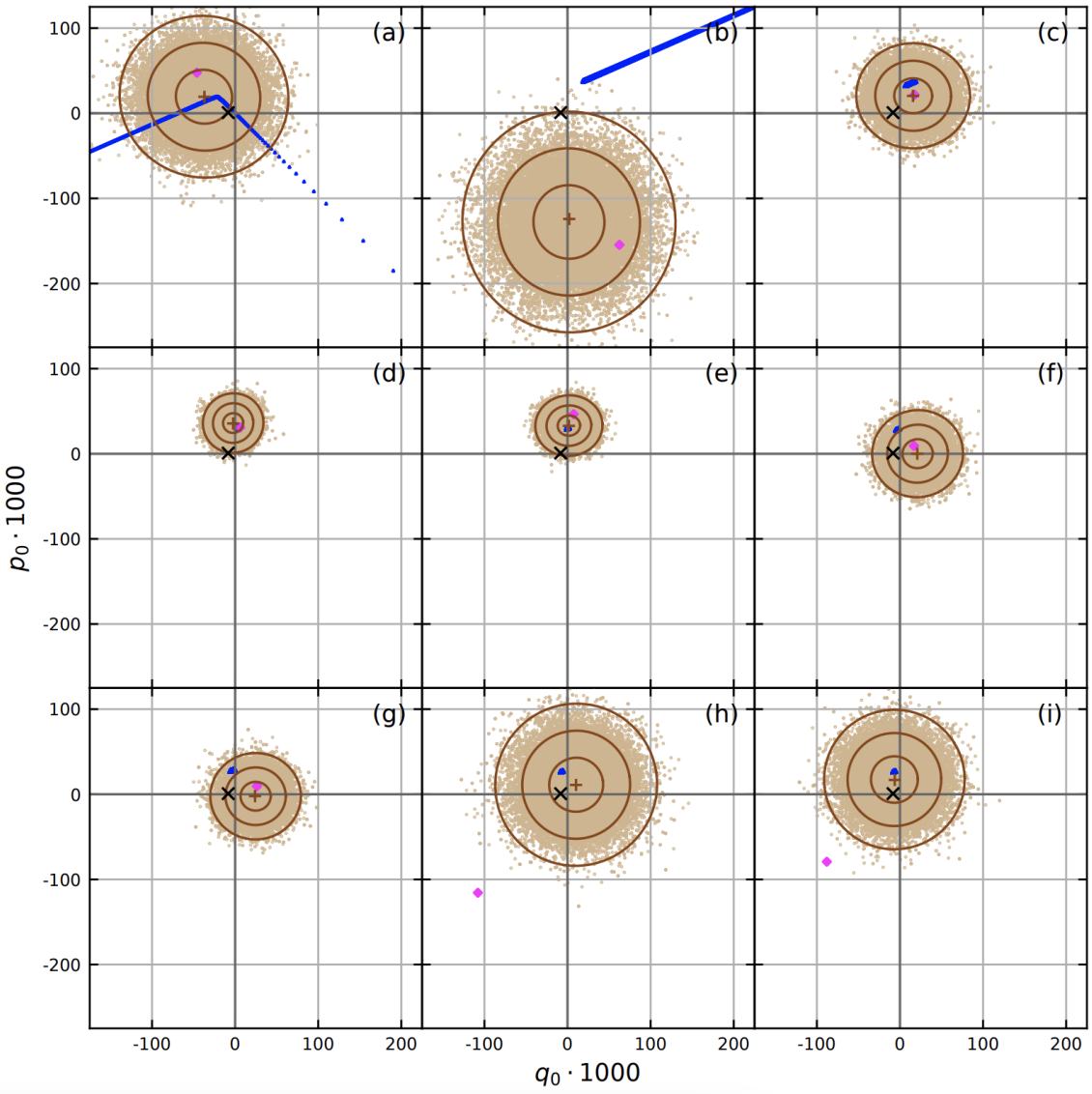

Figure 3. Kuiper Belt midplane confidence ellipses by semimajor axis bin. The best-fit midplane is the brown +. The invariable plane is the black x. The J2000 ecliptic/equinox pole is the origin. The semimajor axis-varying theoretical prediction for the Laplace plane is plotted in blue. The best-fit midplanes of 40,000 random heuristic resamples are in tan, and the 1σ, 2σ, and 3σ covariance ellipses for them are in brown. The best-fit midplane from Volk & Malhotra (2017) is the magenta diamond. Semimajor axis bins are (a) 34.79-40.524 au, (b) 40.524-42 au, (c) 42-43 au, (d) 43-44 au, (e) 44-45 au, (f) 45-48 au, (g) 45-50 au, (h) 50-80 au, and (i) 50-150 au.